ISSN 1330-3651 (Print), ISSN 1848-6339 (Online) https://doi.org/10.17559/TV-20240510001535
Original scientific paper

The Impacts of Air Flow and Leg Geometry on Thermoelectric Generator Performance

Tufan KOÇ, Nevra BAYHAN*

Abstract: In this study, the effect of thermoelectric leg geometry, heat sink and as an innovation, air flow on the performance of Thermoelectric Generators (TEGs) is investigated based on Comsol Multiphysics simulations. For this aim, while a temperature of 350 K was applied to one side of the thermoelectric (TE) module, a heat sink was added to the other side of the module to increase the temperature difference between the surfaces. The studies on thermoelectric generators in the literature have predominantly focused on heat sink geometry, fin structures or materials and module optimization. In this study, contrary to the existing literature, the effect of leg geometry on the electricity generation performance of a thermoelectric generator was analyzed in conjunction with various laminar air flow parameters, and the optimal geometry were determined. Exposing to the same heat source and keeping total volumes of the thermoelectric legs equal is essential to directly observe the effect of leg geometry on electricity generation performance and efficiency. When the results obtained in terms of electricity generation are compared to the rectangular leg structure which is most used in TE modules, it is seen that the TEGs with cylindrical, truncated prism, inverse truncated prism, truncated cone and inverse truncated cone legs produce approximately 9.69%, 14.68%, 16.74%, 12.9% and 19.97% electricity, respectively. When compared in terms of efficiency, it was concluded that the inverse truncated cone was 22.26% more successful than the conventional rectangular leg geometry.

Keywords: frustum prism; inverse conic; inverse prism; leg geometry; thermoelectric generator; truncated conic

1 INTRODUCTION

The ever-increasing demand for energy and limited resources have led scientists to search for alternative energy sources [1, 2]. Thermoelectric modules can be used both as thermoelectric coolers (TEC) and as thermoelectric generators (TEG) [3-5]. Thermoelectric generators, which have many features such as having no moving parts, long life and low maintenance costs, are among the prominent alternative energy sources [5, 6]. Thanks to these features, thermoelectric modules are used in many industrial areas such as waste heat electricity generation [7], body heat electricity generation [8], health sector [4], aviation and space sector [9]. TEGs are solid-state devices operating with the Seebeck effect. They can generate electricity by creating a temperature difference between the module surfaces [5]. However, TEGs are still not at the desired level in terms of efficiency. In the literature, it is possible to carry out the studies on increasing the efficiency level into three categories as TEG system architecture [6], thermoelectric (TE) module leg structure and TE module material structure [10, 11]. Lamba et al. analysed the thermodynamic effect of two different leg structures using the Thomson effect [12]. As a result of this study, they showed that the trapezoidal leg structure was more successful in terms of energy efficiency than the straight leg structure [12]. Maduabuchi et al. compared the X-leg geometry solar thermoelectric generator with conventional rectangular leg structure thermoelectric generator modules and showed that the X-leg geometry structure provides a higher temperature gradient [13]. Karana et al. created an asymmetric and segmented structure for thermoelectric legs and the result they obtained was about 5% in terms of efficiency compared to the classical structure [14]. Bian et al. proposed a design concept of geometry of 3D printing TE legs for radioisotope TEG [15]. They investigated square, cylinder, helix and spoke leg structures and showed that helix and spoke leg structures are more successful than other leg structures both experimentally and practically [15]. Khalil et al. compared the output power values by considering five different TE leg structures. They showed that the most successful of the five different leg geometries was the classical rectangular leg structure [16]. Doraghi et al. analysed three different TE leg structures. These were the rectangular, diamond and cone leg structures. They concluded that the diamond-cut leg structure was more successful than the rectangular leg structure in terms of energy generation [17]. Ge et al. used genetic algorithm (GA) and particle swarm optimization (PSO) to find the optimal leg structure and reported the results for six different leg geometries [18]. Aljaghtham investigated eight different TE leg geometries and showed that although the most successful TE leg structure in terms of energy production is the butterfly TE leg structure, the lowest leg structure in terms of thermal stress is the classical square leg structure [19]. Wang et al. shown that for TE leg structures with different geometrical structures, energy production gains of up to 9.67% can be achieved by reducing the internal resistance and increasing the volume [20]. Erturun et al. analysed four different TE leg structures using the finite element method and showed the effects of the TE leg structure on thermoelectric power generation through experimental and simulations [21]. Rjafallah et al. considered six different geometries of TE legs and investigated a total of twelve different TE leg geometries by creating a hole inside these legs and showed that the square hollow structure was the most successful leg structure [22]. Hasan et al. investigated different geometric TE leg structures by varying the length of the legs and showed that the most successful leg structure was the conical leg structure [23]. Ibeagwu considered five different TE leg geometries and showed that the X-leg structure is the most power generating leg structure with 19.12% [24].

One of the important features of thermoelectric modules is that the waste heat generated during the operation of a system can be reused for power generation [25]. Kumar et al. investigated the performance of thermoelectric generators using three different heat dissipation models and showed that the most successful leg structure is the rectangular leg [26]. Faisal et al. carried out an experimental and simulation study to utilize the waste heat from trucks for TEGs [27]. Mohammed A. et al. used a TEG panel consisting of 15 × 10 TEG modules to convert

waste heat from solar hot water pipes into electricity [28]. Li et al. developed a waste heat TEG using 24 TE modules and produced 96.6 W of electrical power with a pressure drop of 375 Pa at an exhaust gas temperature of 648 K compared to previous models [29]. Ziolkowski et al. worked on electricity generation with jet engine waste and showed that this study will be successful for TE modules with a figure of merit (Z) value greater than two [30]. Thermoelectric legs are very small elements with a size of 1.6 × 1.4 mm. These leg structures, which are generally rectangular in shape for ease of fabrication, are used as both thermoelectric generators and thermoelectric coolers. However, with the development of 3D printing technology, thermoelectric leg structures of different shapes are being produced and used in industry [15, 31]. Thus, studies on the manufacturing of conical TE legs, which are more successful in terms of electricity generation, have gained great importance.

In this study, the effects of thermoelectric leg geometries such as rectangular, cylindrical, truncated prism, inverse truncated prism, truncated cone and inverse truncated cone, heat sink and air velocity on TEG performance were investigated based on Comsol Multiphysics simulation by applying a constant 350 K temperature to the hot surface. However, unlike other studies in the literature, a heat sink was added to the cold side of the TE module to compare the performance of the studied legs and air was supplied over the heat sink to further increase the temperature difference. Under these conditions, the effects of six different leg geometries on the power generation performance of the TEG and simulation results are compared. In order to observe how the leg geometry affects the power generation performance, the total volume of the thermoelectric legs must be kept equal.

This study is structured as follows: The methodologies of TE leg geometries in the form of rectangular, cylinder, truncated prism, inverse truncated prism, truncated cone and inverse truncated cone are explained in section 2. Simulation results on the electricity generation performance of TEG for six different leg geometries are given in section 3. Some concluding remarks are discussed in the last section.

2 METHODOLOGY

2.1 Model Desing and Studied Leg Geometries

A thermoelectric generator (TEG) is a device that uses the Seebeck effect to directly convert heat into electricity. Electricity is generated when a temperature differential is applied, as the mobile charge carriers in the TE elements at the hot-end move to the cold-end. The hot and cold side of the TEG can be changed according to the designer's aim. The purpose of this study is to assess and compare TEG's performance employing legs with different geometry. COMSOL Multiphysics (CMP) was used in all simulations for this purpose. Fig. 1 shows a classical TEG with 128 *p-n* pairs.

The six different TEG leg geometries used in this study are shown in Fig. 2. In order to obtain fast simulation results, the models were simplified, and the study was carried out on two legs (*p-n*). TEGs with two legs that are developed using these geometries are shown in Fig. 2

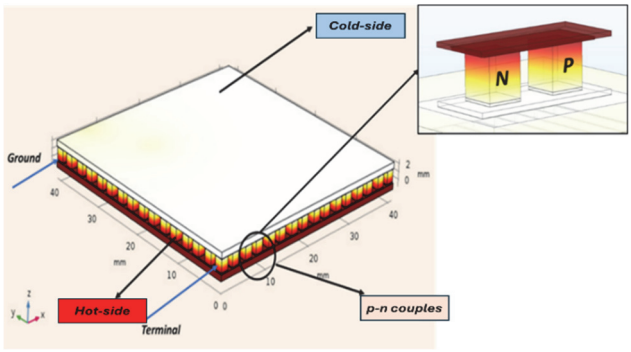

Figure 1 A simple TEG structure

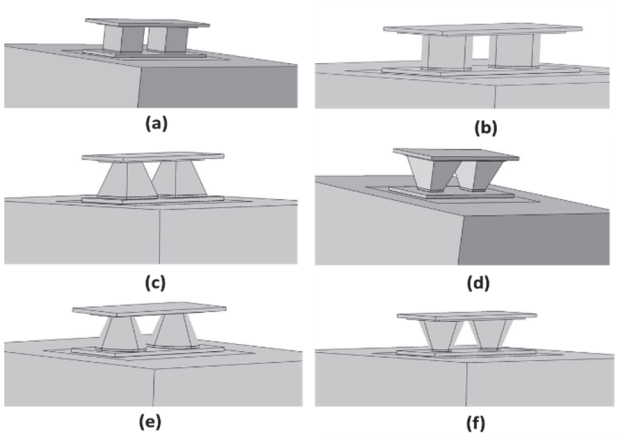

Figure 2 Six different TE leg geometries. (a) Rectangular leg, (b) Cylinder leg, (c) Truncated prism leg, (d) Inverse truncated prism leg, (e) Truncated cone leg, (f) Inverse truncated cone leg

Fig. 3 shows a schematic of the TEG system. Two thermoelectric compounds, Sb2Te3-p and Bi2Te3-n, make up the TEG system. All elements affecting the performance of the TEG have been taken into account in order to obtain realistic simulation results. For example, the parameters of the 55n-95Pb solder paste are taken into account for heat transfer and electrical conductivity between the TE legs and the copper plate, while the physical parameters of the copper are taken into account to ensure electrical conductivity between the semiconductor legs. To optimise heat transfer between the heat sink and the module plate, the simulation has also taken into account the physical properties of a silicone-based thermal grease. The properties of the materials numbered (1) - (6) used in the thermoelectric module in Fig. 3 are shown in Tab. 1.

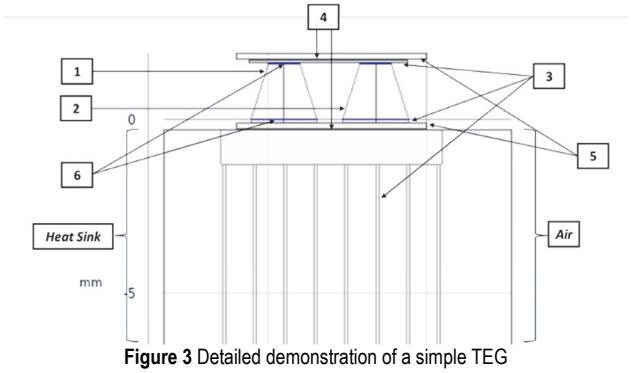

Figure 3 Detailed demonstration of a simple TEG

Fig. 4 shows the structure used in the simulations for the thermoelectric generator.

Table 1 TE material properties

Property	Sb2Te3 (1)	Bi2Te3 (2)	Copper (3)	Alumina (4)	Thermal grease (5)	5Sn-95Pb (6)
Relative permittivity	1	1	1	-	-	1
Density / kg/m^3	6500	7790	8960	3900	2600	rho_liquid_2(T(1/K))
Heat capacity / J/(kg·K)	154	154	385	900	1200	C(T(1/K))
Seebeck coefficient / V/K	200e–6	–220e–6	-	-	-	N/A
Electrical conductivity / S/m	120000	120000	5.998e7	-	-	sigma (T(1/K))
Thermal conductivity / W/(m·K)	1.5	1.5	400	17	3	0.28

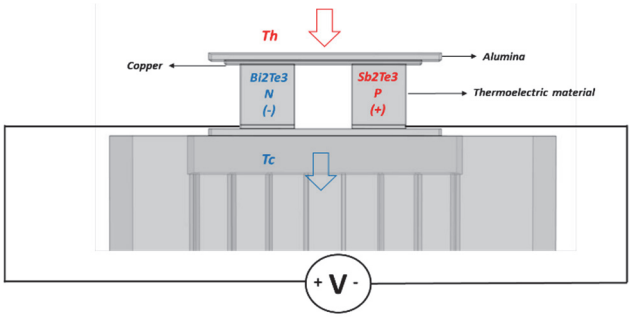

Figure 4 Structure of TEG

Fig. 5 shows the hot side, cold side and air flow direction of the module. The air flow is used to reduce the cold side temperature of the module by entering between the heat sink fins and to increase the temperature gradient. Also, the direction in which the air enters and exits is shown in the Fig. 5. The section where the thermoelectric legs are located is considered to be an isolated environment with no flow.

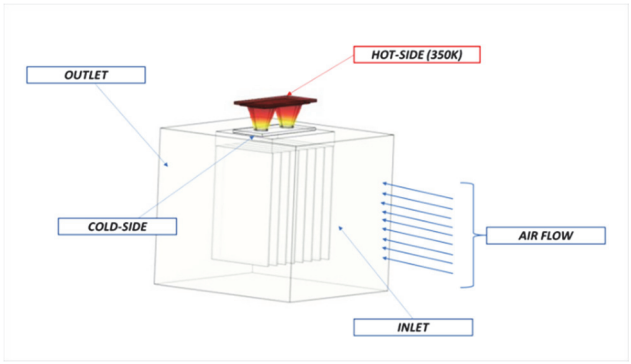

Figure 5 Air flow direction in simulation and boundary conditions

Fig. 6 shows the thermoelectric legs, the isolatearea and the air flow applied to the heat sink. Fig. 6a shows the air flow direction and applied values and Fig. 6b shows the heat distribution where the air flow leaves the heat sink. In Fig. 6, 1 m/s was applied to the simulation as air flow velocity. However, in the study, a total of 15 air flow values from 0.01 m/s to 11 m/s were applied to the system and it was aimed to cool the heat sink and create a thermal gradient between the TE surfaces.

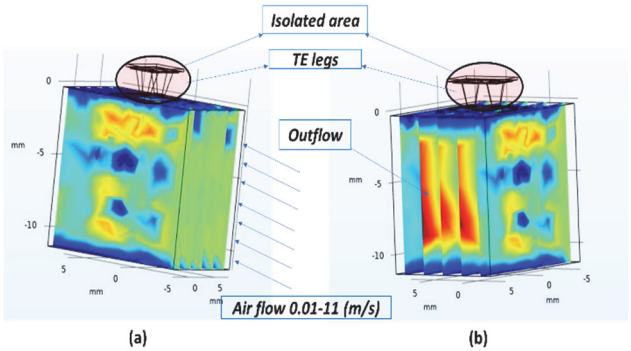

Figure 6 (a) Air flow along the fins of the heat sink, (b) air flow leaves the heat sink

The geometric dimensions of the thermoelectric legs used in simulations are shown in Tab. 2. It is crucial to guarantee that the ensure total volume of the thermoelectric legs remains constant, notwithstanding the variations in their geometries.

Table 2 TE leg dimensions

Leg Shape	Length	Bottom Area	Top Area	Lateral Area	Volume
Rectangular	1.6 mm	1.4 mm × 1.4 mm	1.4 mm × 1.4 mm	8.96 mm^2	3136 mm^3
Cylinder	1.6 mm	r = 0.79 mm	r = 0.79 mm	7.94 mm^2	≅ 3136 mm^3
Truncate of Cone	1.6 mm	r = 1.05 mm	r = 0.497 mm	8.22 mm^2	≅ 3136 mm^3
Truncate of Prism	1.6 mm	1.862 mm × 1.862 mm	0.9 mm × 0.9 mm	9.22 mm^2	≅ 3136 mm^3
Inverse Truncate of Cone	1.6 mm	r = 0.497mm	r = 1.05 mm	8.22 mm^2	≅ 3136 mm^3
Inverse Truncate of Prism	1.6 mm	0.9 mm × 0.9 mm	1.862 mm × 1.862 mm	9.22 mm^2	≅ 3136 mm^3

2.2 Mathematical Equations for TEG

Conduction, convection and radiation are the heat transfer equations needed to explain the system. The definition of conduction heat $(\dot{Q})$ is as follows [32, 33]:

$$\dot{Q} = -kA\frac{\Delta T}{\Delta x} \tag{1}$$

Where, k, A, ΔT and Δx are the heat transfer coefficient, surface area, the temperature difference, and thickness, respectively. The rate of heat transfer through conduction per unit of time is calculated using the Fourier equation. Convection is expressed by Newton's law of cooling, which is demonstrated in Eq. (2).

$$\dot{Q} = hA\left(T_s - T_\infty\right) \tag{2}$$

Where the heat transfer coefficient, the surface area in contact with the fluid surface, the surface temperature, and

the fluid temperature are represented, respectively, by the variables h, A_s, T_s and T_∞. The equation for radiation, the last heat transfer mechanism, is given below [33].

$$\dot{Q} = \varepsilon \left| o \, A_s \left(T_s^4 - T_{am}^4 \right) \right. \tag{3}$$

where ε, A_s, T_s, $\left| o \right.$ and T_{am} are surface emissivity, surface area, the Stefan-Boltzmann constant, absolute temperature of the surface and ambient temperature, respectively. The last formula named the Stefan-Boltzmann equation gives an estimate of the radiant energy emitted from a surface.

This study aims to investigate the steady-state performance of a TEG device. The models are simplified based on the following assumptions:

- Heat transfer has only one dimension.
- All surfaces except the top (hot) and bottom (cold) surfaces are considered thermally insulated (see Fig. 6).
- Thermoelectric elements are connected in parallel thermally and in series electrically.
- Gravity and the buoyancy effects are neglected to reduce simulation times.

2.3 Finite Element Analysis

The simulations are carried out using COMSOL Multiphysics Programme (CMP) based on the heat transfer equations summarized in Eq. (1) to Eq. (3). The list of governing equations is given below respectively [18].

$$\rho C_p u \frac{\partial T}{\partial t} + \nabla q = Q + Q_{td} \tag{4}$$

where ρ, C_p, u, T and Q_{td} are density, the specific heat capacity at constant stress, the velocity vector of translational motion, absolute temperature and thermoelastic damping per unit volume, respectively.

Energy conversion equation is as follows:

$$\nabla \left(\kappa \nabla T \right) - TJ \frac{\partial S}{\partial T} T + \rho J = 0 \tag{5}$$

where J is the current density, S is the Seebeck coefficent. At steady-state conditions, the disturbance of temperature and electric charge is stable. Other important equations utilized in the AC/DC module during the simulation include the following ones:

$$\nabla J = 0 \tag{6}$$

$$E = \nabla V \tag{7}$$

$$J = \sigma \left(E - S \cdot \nabla T \right) \tag{8}$$

where E defines the electrical field and σ is electrical conductivity. For Peltier power and Peltier coefficent as follows:

$$q_p = Q_j \tag{9}$$

$$P = ST \tag{10}$$

where q_p and P are the Peltier heat or power and the Peltier coefficient, respectively. The coefficient of heat transfer for the air in the system should be determined using the Eq. (11) in [34] before the simulation starts.

$$h_{air} = \frac{k_{air} Nu}{L_{fin}} \tag{11}$$

where Nu, L_{fin}, h_{air} and k_{air} are the Nusselt number, the heat sink fin width, the air transfer coefficient and the air's thermal conductivity, respectively. The following relation is used to calculate the Nusselt number [34]:

$$Nu = 0.664 \, Re^{1/2} \, Pr^{1/3} \tag{12}$$

where Re and Pr are the Reynold number and Prandtl number, respectively. The Reynold's number is calculated as follows [34].

$$Re = \frac{U_{air} L_{fin}}{v_{air}} \tag{13}$$

where U_{air}, v_{air} and L_{fin} are the speed of the air, the viscosity of the air and the width of the heat sink fins. Since the calculated Reynold's number is smaller than the four over ten term and since the plate is used as heat sink, Eq. (12) is used for the Nusselt number.

Additionally, the length or thickness of the heat sink fins do not alter the heat transfer coefficient value of the air, as shown in Eq. (11) to Eq. (13). The values of the air transfer coefficient (h_{air}) depend on the fin length and air speed. But since the fin length is fixed in this study, the only factor that alters the air transfer coefficient is air speed, the results of which are displayed in Tab. 3 [34].

Table 3 Air velocity entering the heat sink

Air speed-U / m/s	h_{air} / W/m^{2}K
0.01	5.38
0.1	17.04
0.5	38.11
0.8	48.208
1	53.898
2	77.103
3	93.354
4	107.796
5	120.52
6	132.023
7	142.602
8	152.447
9	161.695
10	170.442
11	178.76

Additionally, the dimensionless figure of merit (Z) is a crucial factor to consider when comparing the performance of TEGs and is given below [11]:

$$Z = \frac{\left(S_p - S_n \right)^2 T_{am}}{\left(\sqrt{k_p \rho_p} + \sqrt{k_n \rho_n} \right)^2} \tag{14}$$

where T_{am}, k, ρ and S are the ambient temperature, the thermal conductivity, the electrical resistance and the Seebeck coefficient, respectively. The sub-indices p and n represent p-type and n-type semiconductors.

$$\eta = \frac{(T_h - T_c)}{T_h} \frac{(1+ZT_m)^{1/2} - 1}{(1+ZT_m)^{1/2} + \frac{T_c}{T_h}} \tag{15}$$

where η, T_h, T_c and T_m are efficiency, the hot side temperature, the cold side temperature and the mean temperature, respectively. The efficiency values (η) will be calculated for six TE leg structures in the following section.

In the next section, the simulation results obtained for six different thermoelectric leg geometries are shown.

3 SIMULATION RESULTS AND DISCUSSION

In this section the Comsol Multiphysics simulation results of the TEGs obtained as rectangular, cylinder, truncated prism, inverse truncated prism, truncated cone and inverse truncated cone are explained in detail, respectively.

The voltage results obtained by applying fifteen different air flow values to the TEG system with the most used rectangular and cylindrical leg structures are compared in Fig. 7.

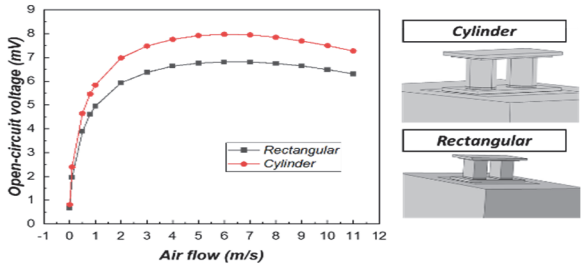

Figure 7 Comparison of the voltages of TEGs with rectangular and cylindrical leg geometry

As seen in Fig. 7, the open-circuit voltage is higher in the cylindrical leg-based module in compared to rectangular leg-based module. This is because the cylindrical module has a surface area that is more exposed to the temperature gradient.

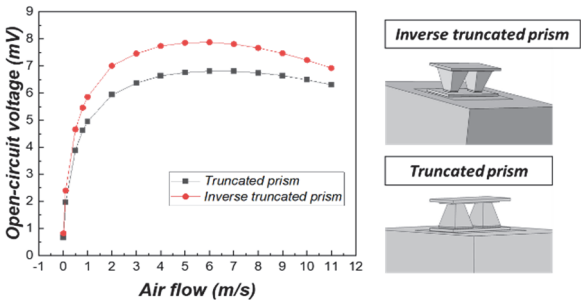

Figure 8 Comparison of the voltages of TEGs with truncated prism and inverse truncated prism leg geometry

As the air flow velocity increases, the voltage generated also increases, but it reaches saturation at a certain value. This phenomenon is attributed to the heat sink cooling capacity reaching saturation after a certain air flow velocity. In other words, the temperature gradient induced by the airflow saturates and remains constant beyond a specific air flow velocity.

The voltage gain results of the TEGs with the truncated prism and inverse truncated prism leg structures are shown in Fig. 8.

The TEG with inverse truncated prism leg generates more open circuit voltage as shown in Fig. 8. This situation can be attributed to the fact that the contact surface of the TE leg with the heat source is higher in the inverse prism structure. In other words, the broad surface in the inverse prism leg structure absorbs more heat energy by contacting the heat source. Therefore, it leads to the activation of more charged particles, resulting in the generation of more open-circuit voltage. The voltage results of the TEGs with the truncated cone and inverse truncated cone leg structures are shown in Fig. 9.

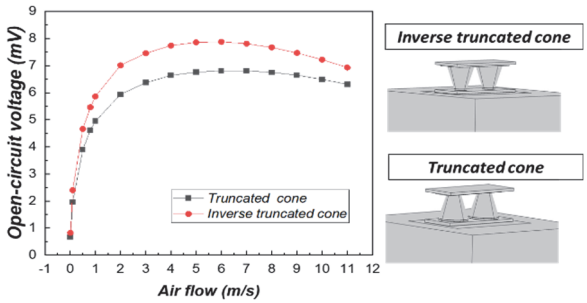

Figure 9 Comparison of the voltages of TEGs with truncated cone and inverse truncated cone leg geometry

A similar situation holds on the TEG with an inverse truncated cone leg. Due to the larger surface area in contact with the heat source, the TE module with an inverse truncated cone leg produces more open-circuit voltage. The comparison of the voltages produced by TEGs with sharp-edged leg geometry such as rectangular, truncated prism and inverse truncated prism is shown in Fig. 10.

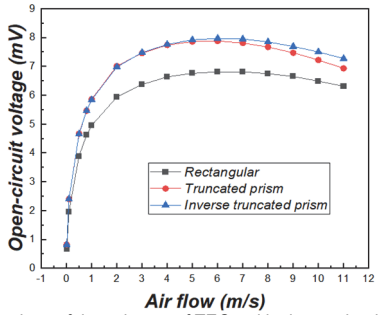

Figure 10 Comparison of the voltages of TEGs with sharp-edged leg geometries

As seen in Fig. 10, the module composed of TE legs with inverse truncated prism geometry produces more voltage than the module with a truncated prism structure. This situation is related to the surface area. The increase in the surface area in contact with the heat source will lead to the stimulation of more charged particles, resulting in more voltage being generated. The comparison of the voltages produced by TEGs with oval-edged leg geometry such as cylinder, truncated cone and inverse truncated cone is shown in Fig. 11.

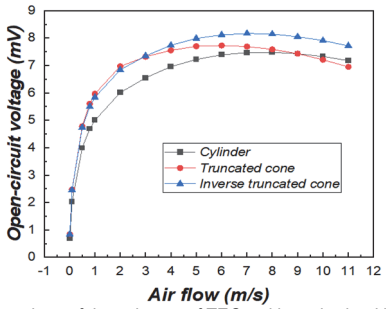

Figure 11 Comparison of the voltages of TEGs with oval-edged leg geometries

As seen in Fig. 11, the module composed of TE legs with inverse truncated cone geometry produces more voltage than the module with a truncated cone structure.

All leg structures studied are compared in terms of open circuit voltage gain in Fig. 12.

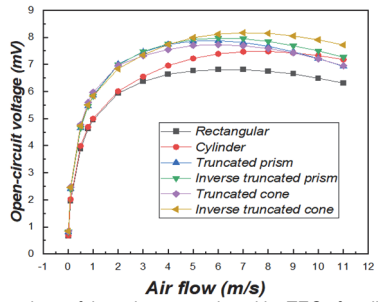

Figure 12 Comparison of the voltages produced by TEGs for all leg geometries

When all leg structures are compared in terms of electricity produced, it can be seen from Fig. 12 that inverse leg structures (inverse truncated cone and inverse truncated prism) are more successful in terms of open circuit voltage gain.

A comparison of the temperature gradients resulting from the air flow speed for TE modules with six different leg geometries exposed to the same heat source (350 K) is shown in Fig. 13. It can be seen from Fig. 13 that the maximum temperature difference occurs for the TEG with inverse truncated cone leg. The lowest temperature gradient is achieved in the TE module with a rectangular leg geometry.

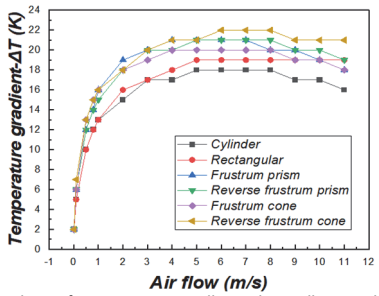

Figure 13 Comparison of temperature gradients depending on air flow speed for six leg geometries

The efficiency values calculated based on six different leg geometries are shown in Fig. 14. Here, the efficiency values are calculated using Eq. (14) and Eq. (15). However, it should be noted that the Z value is not dependent on the geometric structure of the legs and remains the same for all module configurations. Therefore, the fundamental parameter causing the difference in efficiency values in Eq. (14) and Eq. (15) is the temperature gradient. As mentioned earlier, since the temperature gradient is especially directly related to the surface area in contact with the heat source, it is natural for this difference to emerge in efficiency. It can be seen from Fig. 14 that TE modules with inverse conical and inverse prism legs structures achieve the highest efficiency values.

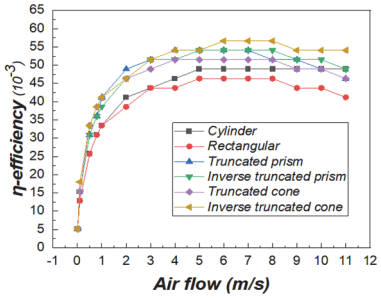

Figure 14 Comparison of the efficiencies for six leg geometries

In this study, a heat sink was added to the cold side of the module to create a temperature gradient at the top and bottom of the TE legs, and an airflow was added to cool the heat sink. It is understood from the simulation results in Fig. 15 that the system is cost-effective. Fig. 15a shows the voltage gain values without heat sink and airflow, Fig. 15b with heat sink only and Fig. 15c when both heat sink and airflow are included in the system. An inverse truncated cone was used as the example leg structure and 1 m/s laminar airflow was applied to the heat sink fins in Fig. 15c.

The voltage gain and efficiency values of the conventional rectangular leg structure, which is the most widely used in TEG systems, and other different five leg geometries are compared in Tab. 4.

The voltage gains obtained when 7 m/s air flow is applied to the system are rectangle 6.81 mV, cylinder 7.47 mV, truncated prism 7.81 mV, inverse truncated prism 7.95 mV, truncated cone 7.69 mV, inverse truncated cone 8.17 mV. When the cylindrical, truncated prism, inverse truncated prism, truncated cone and inverse truncated cone leg TEGs are compared with the rectangular leg TEG, which is used as the most common leg structure in the literature, in terms of electricity generation in Tab. 4, it is seen that 9.69%, 14.68%, 16.74%, 12.9% and 19.97% more electricity is generated respectively. The inverse truncated cone is found to be 22.26% more successful than the traditional rectangular leg geometry when compared in terms of efficiency. When Tab. 4 is analyzed, it can be seen that the most successful TEG leg geometry in terms of both voltage gain, electricity generation and efficiency is the inverse truncated cone.

Various *p*-type and *n*-type leg structures have been used in TEG studies to increase power generation. Some of them are sectional, butterfly, cross-horizontal, I-shape, Y-shape, X-shape, trapezoidal, helix-shape, diamond-shape and hollow [17-23]. For a meaningful comparison, the leg structures used in this study are compared with the same leg structures used in previous studies. As shown in [17, 22, 23], the cone leg structure is more successful than the conventional (rectangular) leg structures in terms of electricity generation.

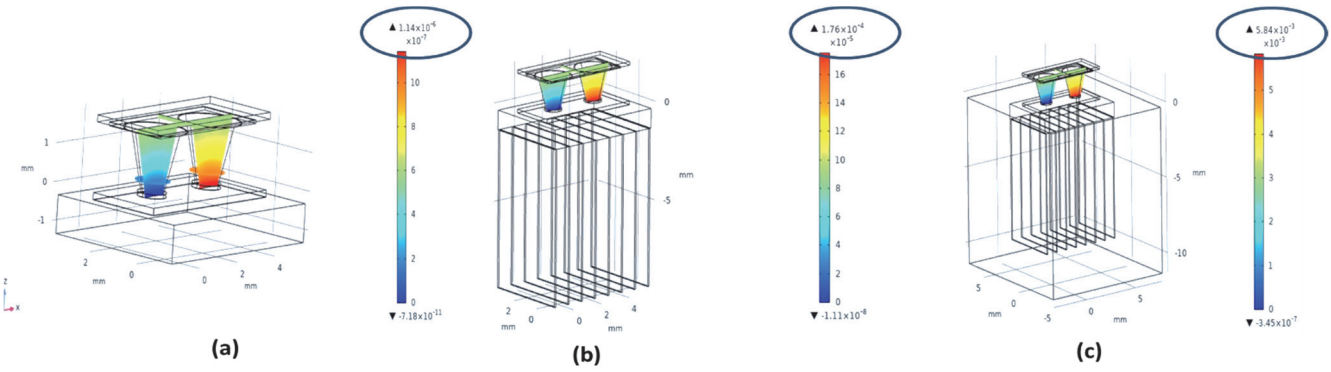

Figure 15 Comparison of three different simulations. (a) system without cooling, (b) system with heat sink, (c) system with heat sink and air flow

Tabel 4 Voltage gain and efficiency comparison for six leg geometries

Leg geometry	Voltage gain / mV	Voltage gain / %	Efficency (10^{-3})	Efficency gain / %
Rectangular	6.81	-	46.35	-
Cylinder	7.47	9.69	48.93	5.56
Truncated prism	7.81	14.68	54.09	16.69
Inverse truncated prism	7.95	16.74	54.09	16.69
Truncated cone	7.69	12.9	51.51	11.13
Inverse truncated cone	8.17	19.97	56.67	22.26

4 CONCLUSION

This study used Comsol Multiphysics simulation to investigate the impacts of air velocity, heat sink, rectangular, cylindrical, truncated prism, inverse truncated prism, truncated cone and inverse truncated cone leg geometries on TEG performance. To evaluate directly how leg geometries affect the efficiency and performance of electricity generation, the TE legs must be exposed to the same heat source and have same total volumes. Laminar air flow was applied into the system to increase the heat sink performance. The examined leg structures have rectangular, cylindrical, truncated prism, inverse truncated prism, truncated cone and inverse truncated cone leg geometries. Unlike the studies in the literature, in this study, an air flow was applied to the cold side of the thermoelectric (TE) module to increase the temperature difference between the surface areas. In order to increase the temperature difference between the surfaces of the module, not only air flow but also a heat sink was used and the temperature value on the cold side of the module was reduced by providing air flow between the heat sink fins.

Six different leg geometries rectangular, cylindrical, truncated prism, inverse truncated prism, truncated cone and inverse truncated cone was examined based on open circuit voltage, efficiency, and airflow velocity. The analyzes especially emphasized the significant impact of the conically shaped geometry on electricity generation performance. It was seen that exposure to the contact surface of the TEG leg with the heat source is higher in the inverse truncated cone structure. Thus, the simulation results indicated that the most successful TEG leg geometry in terms of both voltage gain, electricity generation and efficiency was the inverse truncated cone. Furthermore, it should also be noted that the Z (figure of merit) value is independent of the leg geometry and remains the same for all module configurations.

As an industrial application, the methodology herein can guide the development of solar thermoelectric generators that utilize truncated legs to reduce the volume occupied by rectangular legs in a conventional TEG cell, resulting in lower material requirements and reduced manufacturing cost. In future studies, it is planned to produce TEG modules with different geometric shapes in this study with direct writing 3D printing technology and compare their performances.

5 REFERENCES

[1] Sorrell, S. (2015). Reducing energy demand: A review of issues, challenges and approaches. *Renewable and Sustainable Energy Reviews, 47*, 74-82. https://doi.org/10.1016/j.rser.2015.03.002

[2] Koç, T. & Bayhan, N. (2024). Control of a Thermoelectric Cooling Module by Metaheuristic Optimization Algorithms. *Journal of Aeronautics and Space Technologies, 17*(1), 89-106.

[3] Yusuf, A., Bayhan, N., Tiryaki, H., Hamawandi, B., Toprak, M. S., & Ballikaya, S. (2021). Multi-objective optimization of concen-trated Photovoltaic-Thermoelectric hybrid system via non-dominated sorting genetic algorithm. *Energy Conversion and Management, 236*, 114065. https://doi.org/10.1016/j.enconman.2021.114065

[4] Arikuşu, Y. S. & Bayhan, N. (2024). Design of a Novel PID Controller Based on Machine Learning Algorithm for a Micro-Thermoelectric Cooler of the Polymerase Chain Reaction Device. *IEEE Access, 12,* 61959-61977. https://doi.org/10.1109/ACCESS.2024.3392734

[5] Yusuf, A., Bayhan, N., Ibrahim, A. A., Tiryaki, H., & Ballikaya, S. (2021). Geometric optimization of thermoelectric generator using genetic algorithm considering contact resistance and Thomson effect. *International Journal of Energy Research, 45*(6), 9382-9395. https://doi.org/10.1002/er.6467

[6] Gürkan, K., Karaman, H., & Ballikaya, S. (2023). Optimization of high-performance flexible thermoelectric generator from material synthesis to simulation and device application. *Energy Conversion and Management, 291*, 117335. https://doi.org/10.1016/j.enconman.2023.117335

[7] Liu, X., Deng, Y. D., Li, Z., & Su, C. Q. (2015). Performance analysis of a waste heat recovery thermoelectric generation system for automotive application. *Energy conversion and management, 90*, 121-127. https://doi.org/10.1016/j.enconman.2014.11.015

[8] Hyland, M., Hunter, H., Liu, J., Veety, E., & Vashaee, D. (2016). Wearable thermoelectric generators for human body heat harvesting. *Applied Energy, 182*, 518-524. https://doi.org/10.1016/j.apenergy.2016.08.150

[9] Freer, R. & Powell, A. V. (2020). Realising the potential of thermoelectric technology: A Roadmap. *Journal of Materials Chemistry C, 8*(2), 441-463. https://doi.org/10.1039/C9TC05710B

[10] Ballikaya, S., Chi, H., Salvador, J. R., & Uher, C. (2013) Thermoelectric properties of Ag-doped Cu 2 Se and Cu 2 Te. *Journal of Materials Chemistry A, 1*(40), 12478. https://doi.org/10.1039/C3TA12508D

[11] Ahn, K., Han, M. K., He, J., Androulakis, J., Ballikaya, S., Uher, C., & Kanatzidis, M. G. (2010). Exploring resonance levels and nanostructuring in the PbTe CdTe system and enhancement of the thermoelectric figure of merit. *Journal of the American Chemical Society, 132*(14), 5227-5235. https://doi.org/10.1021/ja910762q

[12] Lamba, R. & Kaushik, S. C. (2017). Thermodynamic analysis of thermoelectric generator including influence of Thomson effect and leg geometry configuration. *Energy Conversion and Management, 144*, 388-398. https://doi.org/10.1016/j.enconman.2017.04.069

[13] Maduabuchi, C., Ejenakevwe, K., Jacobs, I., Ndukwe, A., & Mgbemene, C. (2020). Analysis of a two-stage variable leg geometry solar thermoelectric generator. In *2nd African International Conference on Industrial Engineering and Operations Management*, 1-7.

[14] Karana, D. R. & Sahoo, R. R. (2019). Influence of geometric parameter on the performance of a new asymmetrical and segmented thermoelectric generator. *Energy, 179*, 90-99. https://doi.org/10.1016/j.energy.2019.04.199

[15] Bian, M., Xu, Z., Meng, C., Zhao, H., & Tang, X. (2022). Novel geometric design of thermoelectric leg based on 3D printing for radioisotope thermoelectric generator. *Applied Thermal Engineering, 212*, 118514. https://doi.org/10.1016/j.applthermaleng.2022.118514

[16] Khalil, A., Elhassnaoui, A., Yadir, S., Abdellatif, O., Errami, Y., & Sahnoun, S. (2021). Performance comparison of TEGs for diverse variable leg geometry with the same leg volume. *Energy, 224*, 119967. https://doi.org/10.1016/j.energy.2021.119967

[17] Doraghi, Q., Khordehgah, N., Żabnieńska-Góra, A., Ahmad, L., Norman, L., Ahmad, D., & Jouhara, H. (2021). Investigation and computational modelling of variable teg leg geometries. *Chem. Engineering, 5*(3), 45. https://doi.org/10.3390/chemengineering5030045

[18] Ge, Y., He, K., Xiao, L., Yuan, W., & Huang, S. M. (2022). Geometric optimization for the thermoelectric generator with variable cross-section legs by coupling finite element method and optimization algorithm. *Renewable Energy, 183*, 294-303. https://doi.org/10.1016/j.renene.2021.11.016

[19] Aljaghtham, M. (2024). Comparative performance analysis of thermoelectric generators with a novel leg geometries. *Energy Reports, 11*, 859-876. https://doi.org/10.1016/j.egyr.2023.12.041

[20] Wang, P., Wang, B., Wang, K., Gao, R., & Xi, L. (2021). An analytical model for performance prediction and optimization of thermoelectric generators with varied leg cross-sections. *International Journal of Heat and Mass Transfer, 174*, 121292. https://doi.org/10.1016/j.ijheatmasstransfer.2021.121292

[21] Erturun, U., Erermis, K., & Mossi, K. (2014). Effect of various leg geometries on thermo-mechanical and power generation performance of thermoelectric devices. *Applied Thermal Engineering, 73*(1), 128-141. https://doi.org/10.1016/j.applthermaleng.2014.07.027

[22] Rjafallah, A., Cotfas, D. T., & Cotfas, P.A. (2022). Legs Geometry Influence on the Performance of the Thermoelectric Module. *Sustainability, 14*(23), 15823. https://doi.org/10.3390/su142315823

[23] Hasan, M. N. & Ali, M. S. M. (2021). Influence of leg geometry on the performance of Bismuth Telluride-based Thermoelectric Generator. *ELEKTRIKA-Journal of Electrical Engineering, 20*(2-2), 25-29.

[24] Ibeagwu, O. I. (2019). Modelling and comprehensive analysis of TEGs with diverse variable leg geometry. *Energy, 180*(1), 90-106. https://doi.org/10.1016/j.energy.2019.05.088

[25] Rowe, D. M. & Min, G. (1998). Evaluation of thermoelectric modules for power generations. *Journal of Power Sources, 73*(2), 193-198. https://doi.org/10.1016/S0378-7753(97)02801-2

[26] Kumar, R. C., Sonthalia, A., & Goel, R. (2011). Experimental study on waste heat recovery from an IC engine using thermoelectric technology. *Thermal science, 15*(4), 1011-1022. https://doi.org/10.2298/TSCI100518053K

[27] Albatati, F. & Attar, A. (2021). Analytical and experimental study of thermoelectric generator (TEG) system for automotive exhaust waste heat recovery. *Energies, 14*(1), 204. https://doi.org/10.3390/en14010204

[28] Qasim, M. A., Velkin, V. I., & Shcheklein, S. E. (2022). Experimental and Implementation of a 15 × 10 TEG Array of a Thermoelectric Power Generation System Using Two-Pass Flow of a Tap Water Pipeline Based on Renewable Energy. *Applied Sciences, 12*(15), 7948. https://doi.org/10.3390/app12157948

[29] Li, G., Ying, J., Zheng, Y., Guo, W., Tang, Y., & Ye, C. (2022). Analytical design model for waste heat thermoelectric generator and experimental verification. *Energy Conversion and Management, 252*, 115034. https://doi.org/10.1016/j.enconman.2021.115034

[30] Ziolkowski, P., Zabrocki, K., & Müller, E. (2018). TEG design for waste heat recovery at an aviation jet engine nozzle. *Applied Sciences, 8*(12), 2637. https://doi.org/10.3390/app8122637

[31] Kim, K., Choo, S., Lee, J., Ju, H., Jung, S. H., Jo, S., & Son, J. S. (2024). Heat-Dissipation Design and 3D Printing of Ternary Silver Chalcogenide-Based Thermoelectric Legs for Enhancing Power Generation Performance. *Advanced Science, 11*(30), 2402934. https://doi.org/10.1002/advs.202402934

[32] Yusuf, A., Koç, T., Arikuşu, Y. S., Tiryaki, H., Bayhan, N., & Ballikaya, S. (2022). Modeling of a thermoelectric cooler system, design and optimization of the system's controller. *Sādhanā, 47*(3), 182. https://doi.org/10.1007/s12046-022-01954-8

[33] Cengel, Y. A., Klein, S., & Beckman, W. (1998), *Heat transfer: a practical approach*. WBC McGraw-Hill, Boston: USA. ISBN-13: 978-0075611776

[34] Anderson, J. D. (1995). *Computational fluid dynamics the basics with applications.* McGraw-Hill, New York. ISBN 0-07-113210-4

Contact information:

Tufan KOÇ, PhD. Student
National Defence University,
Institute of Atatürk Strategic Studies and Graduate, Istanbul, Turkey
E-mail: tkoc@hho.msu.edu.tr

Nevra BAYHAN, Asst. Prof. PhD.
(Corresponding author)
Istanbul University-Cerrahpaşa,
Department of Electrical and Electronics Engineering,
34320 Istanbul, Turkey
E-mail: nevra@iuc.edu.tr